Injection Laser

The electroluminescent properties of the forward-biased *p–n* junction diode have been considered in the preceding sections. Stimulated emission by the recombination of the injected carriers is encouraged in the semiconductor injection laser (also called the injection laser diode (ILD) or simply the injection laser) by the provision of an optical cavity in the crystal structure in order to provide the feedback of photons. This gives the injection laser several major advantages over other semiconductor sources (e.g. LEDs) that may be used for optical communications. These are as follows:

1. High radiance due to the amplifying effect of stimulated emission. Injection lasers will generally supply milliwatts of optical output power.

2. Narrow linewidth on the order of 1 nm (10 Å) or less which is useful in minimizing the effects of material dispersion.

3. Modulation capabilities which at present extend up into the gigahertz range and will undoubtedly be improved upon.

4. Relative temporal coherence which is considered essential to allow heterodyne (coherent) detection in high-capacity systems, but at present is primarily of use in single-mode systems

5. Good spatial coherence which allows the output to be focused by a lens into a spot which has a greater intensity than the dispersed unfocused emission.

This permits efficient coupling of the optical output power into the fiber even for fibers with low numerical aperture. The spatial fold matching to the

optical fiber which may be obtained with the laser source is not possible with an incoherent emitter and, consequently, coupling efficiencies are much reduced

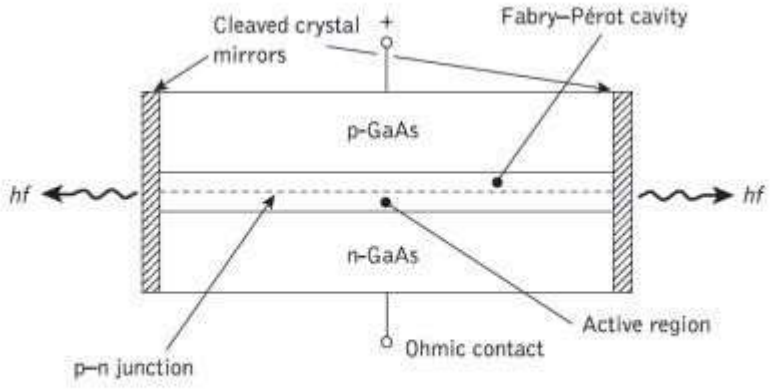

Figure 3.4 Schematic diagram of a GaAs homojunction injection laser with a Fabry–Pérot cavity

[Source: htpp://img.brainkart.com]

These advantages, together with the compatibility of the injection laser with optical fibers (e.g. size), led to the early developments of the device in the 1960s. Early injection lasers had the form of a Fabry–Pérot cavity often fabricated in gallium arsenide which was the major III–V compound semiconductor with electroluminescent properties at the appropriate wavelength for first-generation systems. The basic structure of this homojunction device is shown in Figure 3.4, where the cleaved ends of the crystal act as partial mirrors in order to encourage stimulated emission in the cavity when electrons are injected into the *p*-type region. However, as mentioned previously these devices had a high threshold current density (greater than 104 A cm−2) due to their lack of carrier containment and proved inefficient light sources.

High current densities required dictated that these devices when operated at 300 K were largely utilized in a pulsed mode in order to minimize the junction temperature and thus avert damage. Improved carrier containment and thus lower threshold current densities (around 103 A cm−2) were achieved using heterojunction structures.

The DH injection laser fabricated from lattice-matched III–V alloys provided both carrier and optical confinement on both sides of the *p*–*n* junction, giving the injection laser a greatly enhanced performance. This enabled these devices with the appropriate heat sinking to be operated in a CW mode at 300 K with obvious advantages for optical communications (e.g. analog transmission). However, in order to provide reliable CW operation of the DH injection laser it was necessary to provide further carrier and optical confinement which led to the introduction of stripe geometry DH laser configurations. Prior to discussion of this structure, however, it is useful to consider the efficiency of the semiconductor injection laser as an optical source.

Stripe Geometry

The DH laser structure provides optical confinement in the vertical direction through the refractive index step at the heterojunction interfaces, but lasing takes place across the whole width of the device. This situation is illustrated in Figure 3.5 which shows the broad-area DH laser where the sides of the cavity are simply formed by roughening the edges of the device in order to reduce unwanted emission in these directions and limit the number of horizontal transverse modes. However, the broad emission area creates several problems including difficult heat sinking, lasing from multiple filaments in the relatively wide active area and unsuitable light output geometry for efficient coupling to the cylindrical fibers.

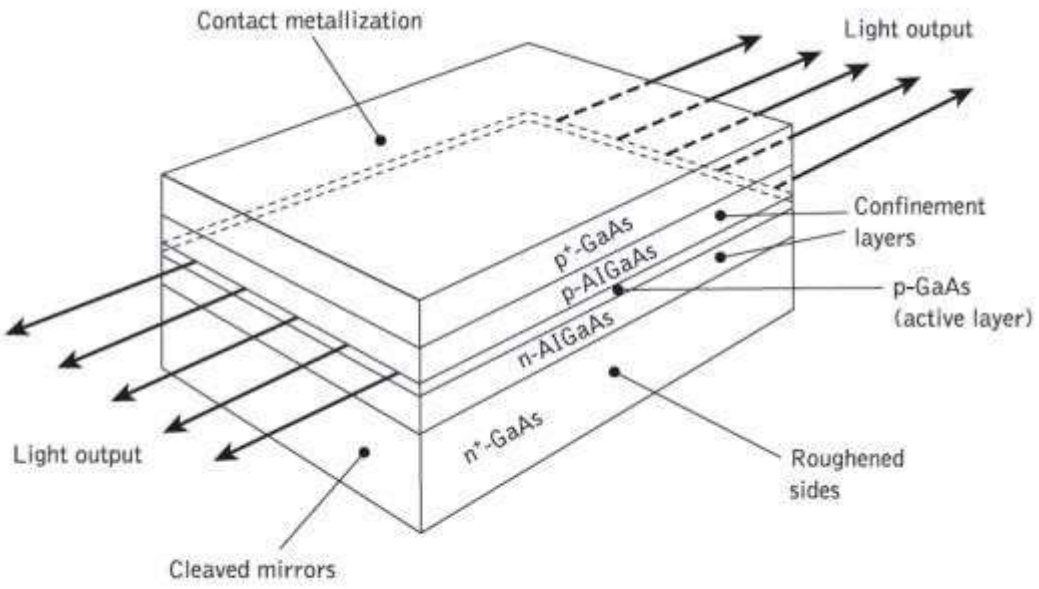

Figure 3.5 A broad-area GaAs/AlGaAs DH injection laser

[Source: htpp://img.brainkart.com]

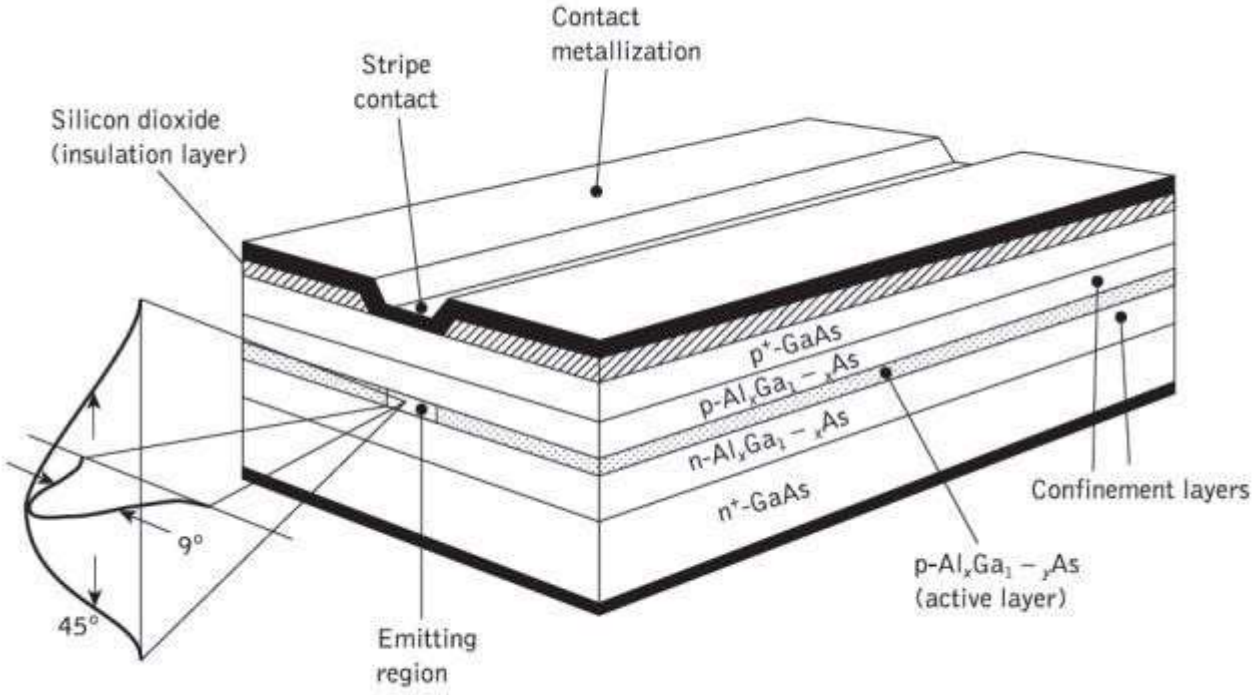

Figure 3.6 Schematic representation of an oxide stripe AlGaAs DH injection laser

[Source: htpp://img.brainkart.com]

To overcome these problems while also reducing the required threshold current, laser structures in which the active region does not extend to the edges of the device were developed. A common technique involved the introduction

of stripe geometry to the structure to provide optical containment in the horizontal plane. The structure of a DH stripe contact laser is shown in Figure 3.6 where the major current flow through the device and hence the active region is within the stripe. Generally, the stripe is formed by the creation of high-resistance areas on either side by techniques such as proton bombardment or oxide isolation.

The stripe therefore acts as a guiding mechanism which overcomes the major problems of the broad-area device. However, although the active area width is reduced the light output is still not particularly well collimated due to isotropic emission from a small active region and diffraction within the structure. The optical output and far-field emission pattern are also illustrated in Figure 6.21. The output beam divergence is typically 45° perpendicular to the plane of the junction and 9° parallel to it. Nevertheless, this is a substantial improvement on the broad-area laser.

Injection Laser Structures

1. Gain-Guided Lasers.

Fabrication of multimode injection lasers with a single or small number of lateral modes is achieved by the use of stripe geometry. These devices are often called gain-guided lasers. The constriction of the current flow to the stripe is realized in the structure either by implanting the regions outside the stripe with protons (proton isolated stripe) to make them highly resistive, or by oxide or *p–n* junction isolation. The structure for an aluminium gallium arsenide oxide isolated stripe DH laser was shown in Figure 3.6. It has an active region of gallium arsenide bounded on both sides by aluminium gallium arsenide regions. This technique has been widely applied, especially for multimode laser

structures used in the shorter wavelength region. The current is confined by etching a narrow stripe in a silicon dioxide film.

Two other basic techniques for the fabrication of gain-guided laser structures are illustrated in Figure3.7(a) and (b) which show the proton-isolated stripe and the *p–n* junction isolated stripe structures respectively. In Figure 3.7(a) the resistive region formed by the proton bombardment gives better current confinement than the simple oxide stripe and has superior thermal properties due to the absence of the silicon dioxide layer; *p–n* junction isolation involves a selective diffusion through the *n*-type surface region in order to reach the *p*-type layers, as illustrated in Figure 1(b). None of these structures confines all the radiation and current to the stripe region and spreading occurs on both sides of the stripe.

With stripe widths of 10 μm or less, such planar stripe lasers provide highly efficient coupling into multimode fibers, but significantly lower coupling efficiency is achieved into small-core-diameter single-mode fibers. However, with certain practical laser diodes the characteristic is not linear in the simulated emission region, but exhibits kinks. This phenomenon is particularly prevalent with gain-guided injection laser devices. The kinks may be classified into two broad categories.

The first type of kink results from changes in the dominant lateral mode of the laser as the current is changed. The output characteristic for laser *A* in Figure 3.8(a) illustrates this type of kink where lasing from the device changes from the fundamental lateral mode to a higher order lateral mode (second order) in a current region corresponding to a change in slope. The second type of kink involves a ‘spike’, as observed for laser *B* of Figure 3.8(a). These spikes have been shown to be associated with filamentary behaviour within the active region of the device. The filaments result from defects within the crystal structure.

Both these mechanisms affect the near- and far-field intensity distributions (patterns) obtained from the laser. A typical near-field intensity distribution corresponding to a single optical output power level in the plane of the junction is shown in Figure 3.8(b).

As this distribution is in the lateral direction, it is determined by the nature of the lateral waveguide. The single intensity maximum shown indicates that the fundamental lateral mode is dominant. To maintain such a near-field pattern the stripe geometry of the device is important. In general, relatively narrow stripe devices (< 10 μm) formed by a planar process allow the fundamental lateral mode to dominate.

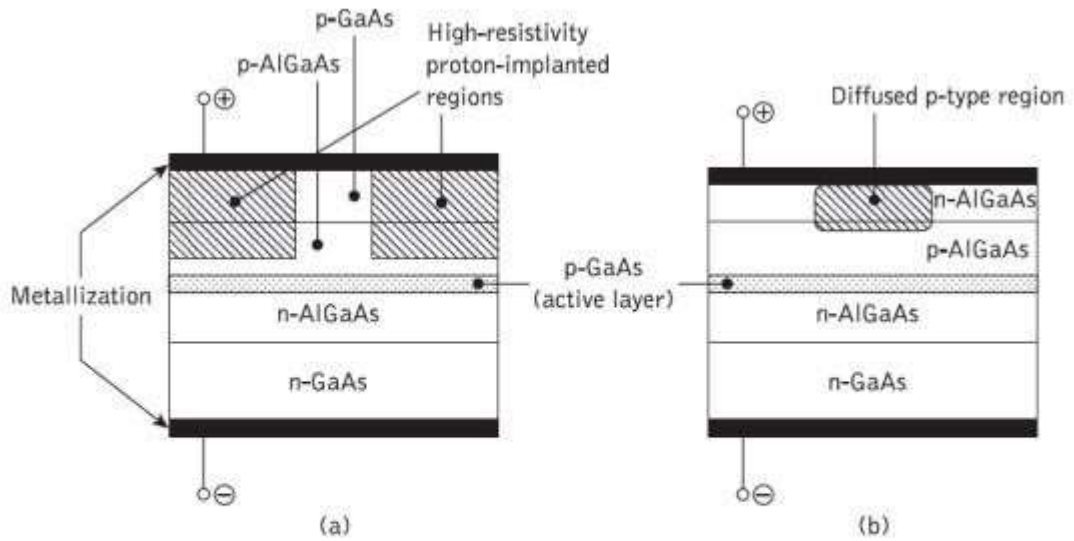

Figure 3.7 Schematic representation of structures for stripe geometry injection lasers: (a) proton-isolated stripe GaAs/AlGaAs laser; (b) *p–n* junction isolated (diffused planar stripe) GaAs/AlGaAs laser

[Source: htpp://img.brainkart.com]

This is especially the case at low power levels where near-field patterns similar to Figure 3.8(b) may be obtained. Although gain-guided lasers are commercially available for operation in both the shorter wavelength range (using GaAs active regions) and the longer wavelength range (using InGaAsP active regions) they exhibit several undesirable characteristics.

Apart from the nonlinearities in the light output versus current characteristics discussed above, gain-guided injection lasers have relatively high threshold currents (100 to 150 mA) as well as low differential quantum efficiency. These effects are primarily caused by the small carrier-induced refractive index reduction within the devices which results in the movement of the optical mode along the junction plane. The problems can be greatly reduced by introducing some real refractive index variation into the lateral structure of the laser such that the optical mode along the junction plane is essentially determined by the device structure.

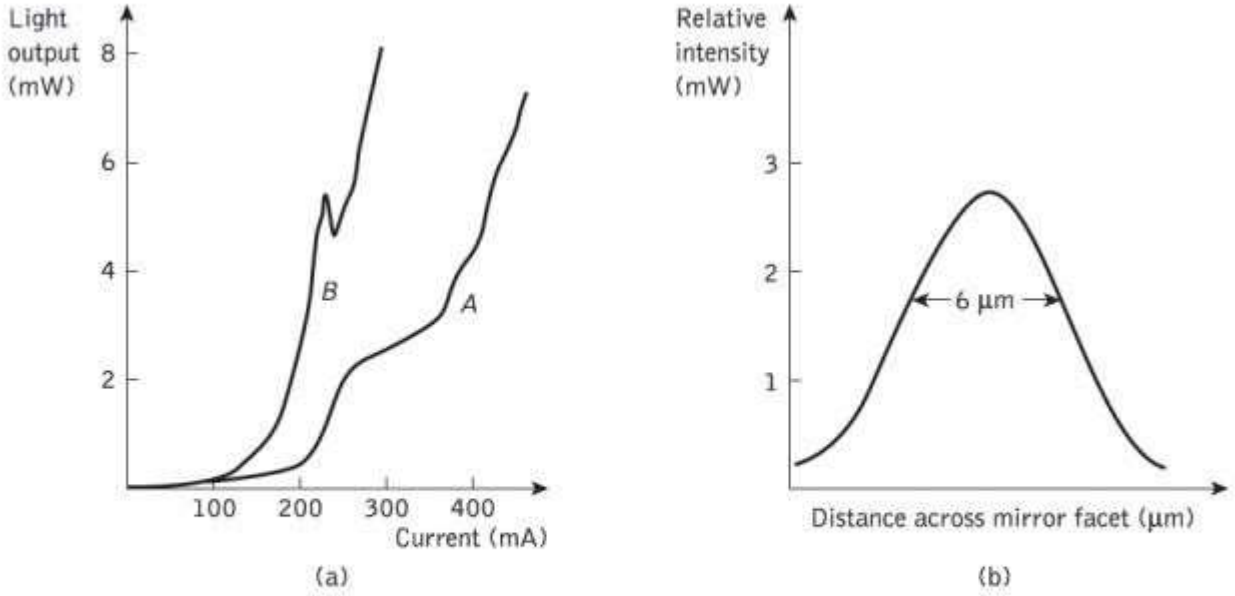

Figure 3.8 (a) The light output against current characteristic for an injection laser with nonlinearities or a kink in the stimulated emission region. (b) A typical near-field intensity distribution (pattern) in the plane of the junction for an injection laser

[Source: htpp://img.brainkart.com]

2. Index-Guided Lasers

The drawbacks associated with the gain-guided laser structures were largely overcome through the development of index-guided injection lasers. In some such structures with weak index guiding, the active region waveguide thickness is varied by growing it over a channel or ridge in the substrate. A ridge is produced above the active region and the surrounding areas are etched

close to it (i.e. within 0.2 to 0.3 μm). Insulating coatings on these surrounding areas confine the current flow through the ridge and active stripe while the edges of the ridge reflect light, guiding it within the active layer, and thus forming a waveguide. Hence in the ridge waveguide laser shown in Figure 3.9 (a), the ridge not only provides the location for the weak index guiding but also acts as the narrow current confining stripe. These devices have been fabricated to operate at various wavelengths with a single lateral mode, and room temperature CW threshold currents as low as 18 mA with output powers of 25 mW have been reported.

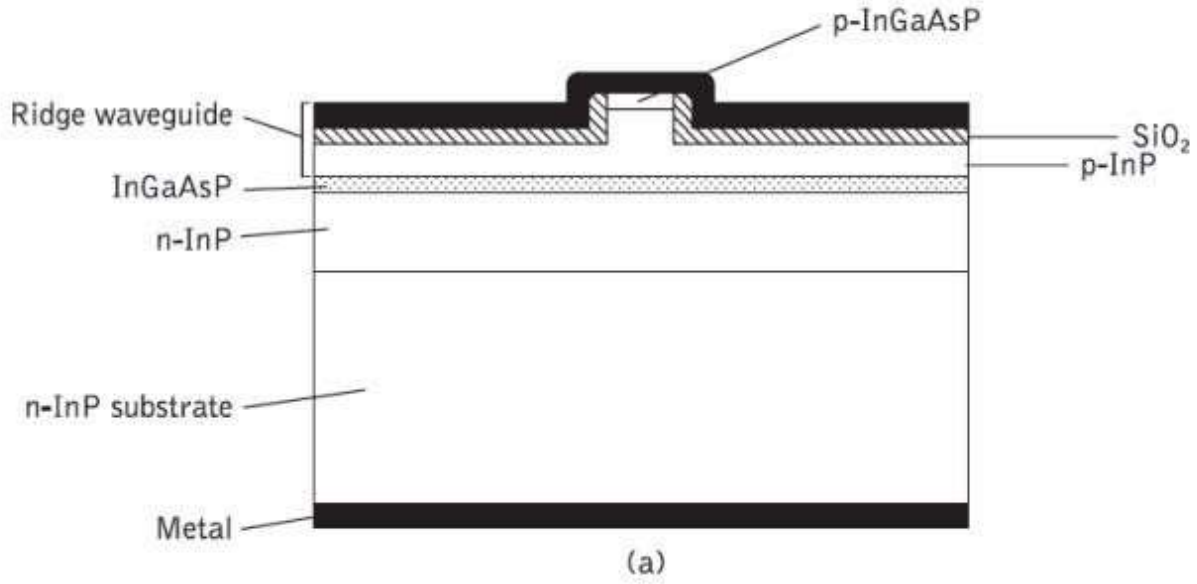

(a)

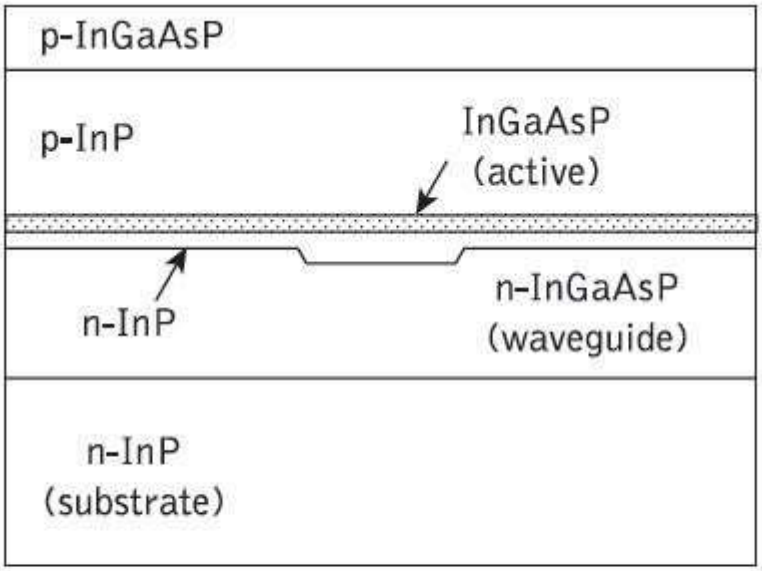

(b)

Figure 3.9 Index-guided lasers: (a) ridge waveguide injection laser structures; (c) rib (plano-convex) waveguide injection laser structure

[Source: htpp://img.brainkart.com]

More typically, the threshold currents for such weakly index-guided structures are in the range 40 to 60 mA, which compares a light output versus current characteristic for a ridge waveguide laser with that of an oxide stripe gain-guided device. Alternatively, the application of a uniformly thick, planar active waveguide can be achieved through lateral variations in the confinement layer thickness or the refractive index. However, room temperature CW threshold currents are between 70 and 90 mA with output powers of around 20 mW for InGaAsP devices operating at a wavelength of 1.3 μm.

3. Quantum-Well Lasers

DH lasers have also been fabricated with very thin active layer thicknesses of around 10 nm instead of the typical range for conventional DH structures of 0.1 to 0.3 μm. The carrier motion normal to the active layer in these devices is restricted, resulting in a quantization of the kinetic energy into

discrete energy levels for the carriers moving in that direction. This effect is similar to the well-known quantum mechanical problem of a one dimensional potential well and therefore these devices are known as quantum well lasers. In this structure the thin active layer causes drastic changes to the electronic and optical properties in comparison with a conventional DH laser.

These changes are due to the quantized nature of the discrete energy levels with a step-like density of states which differs from the continuum normally obtained. Hence, quantum-well lasers exhibit an inherent advantage over conventional DH devices in that they allow high gain at low carrier density, thus providing the possibility of significantly lower threshold currents. Both single-quantum-well (SQW), corresponding to a single active region, and multiquantum-well (MQW), corresponding to multiple active regions, lasers are utilized. In the latter structure, the layers separating the active regions are called barrier layers. Energy band diagrams for the active regions of these structures are displayed in Figure 3.10. It may be observed in Figure 3.10(c) that when the bandgap energy of the barrier layer differs from the cladding layer in an MQW device, it is usually referred to as a modified multiquantum-well laser.

Better confinement of the optical mode is obtained in MQW lasers in comparison with SQW lasers, resulting in a lower threshold current density for these devices. A substantial amount of experimental work has been carried out on MQW lasers using the AlGaAs/GaAs material system. It has demonstrated the superior characteristics of MQW devices over conventional DH lasers in relation to lower threshold currents, narrower line widths, higher modulation speeds, lower frequency chirp and less temperature dependence.

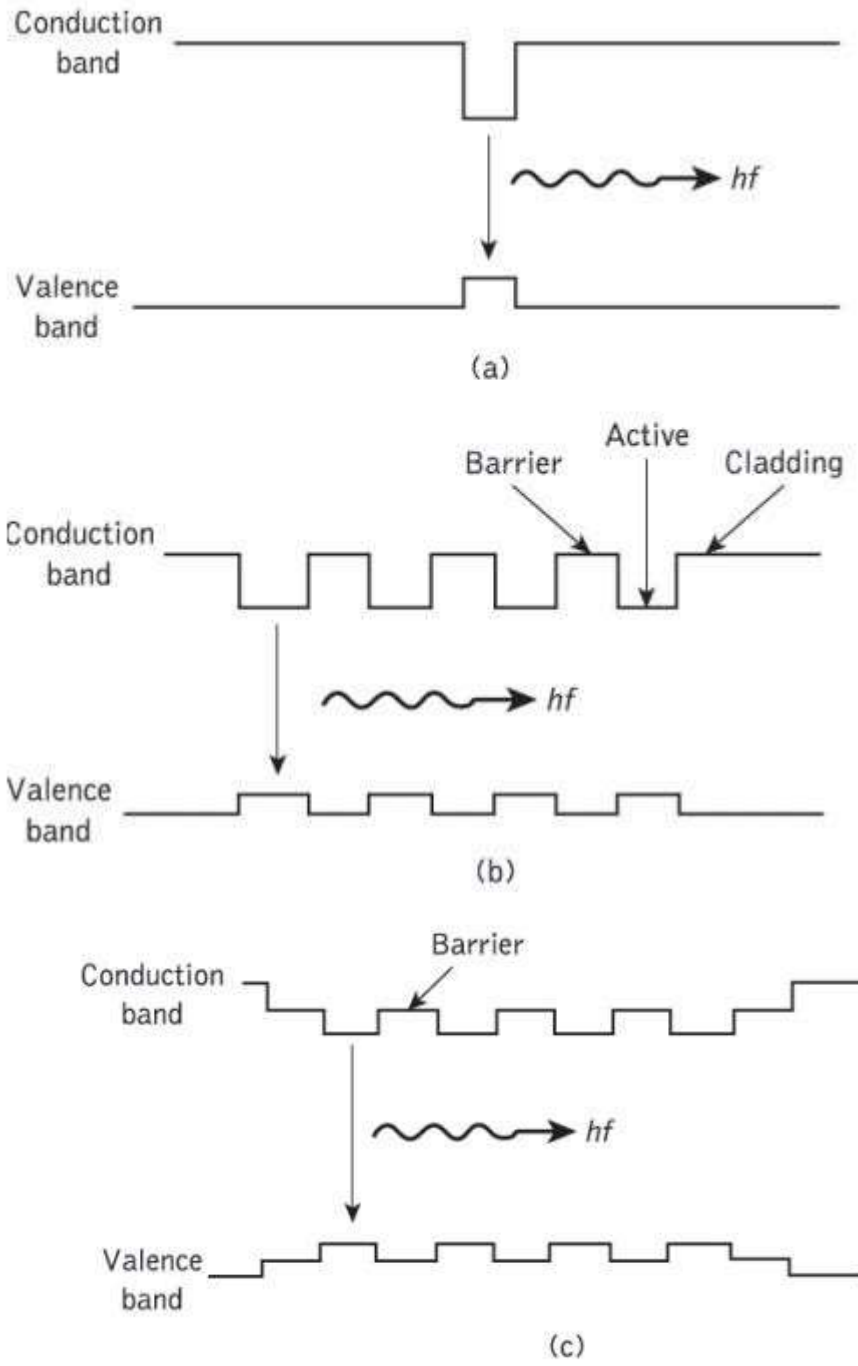

Figure 3.10 Energy band diagrams showing various types of quantum-well structure: (a) single quantum well; (b) multiquantum well; (c) modified multiquantum well

[Source: htpp://img.brainkart.com]

Introduction

The optical source is often considered to be the active component in an optical fiber communication system. Its fundamental function is to convert electrical energy in the form of a current into optical energy (light) in an efficient manner which allows the light output to be effectively launched or coupled into the optical fiber. Three main types of optical light source are available. These are:

- ✓ wideband 'continuous spectra' sources (incandescent lamps)
- ✓ monochromatic incoherent sources (light-emitting diodes, LEDs);
- ✓ monochromatic coherent sources (lasers).

To aid consideration of the sources currently in major use, the historical aspect must be mentioned. In the early stages of optical fiber communications the most powerful narrowband coherent light sources were necessary due to severe attenuation and dispersion in the fibers. Therefore, gas lasers (helium-neon) were utilized initially. However, the development of the semiconductor injection laser and the LED, together with the substantial improvement in the properties of optical fibers, has given prominence to these two specific sources

LEDs

Spontaneous emission of radiation in the visible and infrared regions of the spectrum from a forward-biased *p–n* junction was discussed. The normally empty conduction band of the semiconductor is populated by electrons injected into it by the forward current through the junction, and light is generated when these electrons recombine with holes in the valence band to emit a photon. This is the mechanism by which light is emitted from an LED, but stimulated emission is not encouraged, as it is in the injection laser, by the addition of an optical cavity and mirror facets to provide feedback of photons.

The LED can therefore operate at lower current densities than the injection laser, but the emitted photons have random phases and the device is an incoherent optical source. Also, the energy of the emitted photons is only roughly equal to the band gap energy of the semiconductor material, which gives a much wider spectral line width (possibly by a factor of 100) than the injection laser. The line width for an LED corresponds to a range of photon energy between 1 and 3.5*KT*, where *K* is Boltzmann's constant and *T* is the absolute temperature.

This gives line widths of 30 to 40 nm for GaAs-based devices operating at room temperature. Thus the LED supports many optical modes within its structure and is therefore often used as a multimode source, although the coupling of LEDs to single-mode fibers has been pursued with success, particularly when advanced structures are employed. Also, LEDs have several further drawbacks in comparison with injection lasers.

These include:

- ✓ generally lower optical power coupled into a fiber (microwatts)
- ✓ usually lower modulation bandwidth
- ✓ harmonic distortion.

However, although these problems may initially appear to make the LED a less attractive optical source than the injection laser, the device has a number of distinct advantages which have given it a prominent place in optical fiber communications:

Simpler fabrication. There are no mirror facets and in some structures no striped geometry.

Cost. The simpler construction of the LED leads to much reduced cost which is always likely to be maintained.

Reliability. The LED does not exhibit catastrophic degradation and has proved far less sensitive to gradual degradation than the injection laser. It is also immune to self-pulsation and modal noise problems.

Generally less temperature dependence. The light output against current characteristic is less affected by temperature than the corresponding characteristic for the injection laser. Furthermore, the LED is not a threshold device and therefore raising the temperature does not increase the threshold current above the operating point and hence halt operation.

Simpler drive circuitry. This is due to the generally lower drive currents and reduced temperature dependence which makes temperature compensation circuits unnecessary.

Linearity. Ideally, the LED has a linear light output against current characteristic, unlike the injection laser. This can prove advantageous where analog modulation is concerned.

The planar LED is the simplest of the structures that are available and is fabricated by either liquid- or vapor-phase epitaxial processes over the whole surface of a GaAs substrate. This involves a *p*-type diffusion into the *n*-type substrate in order to create the junction illustrated in Figure 3.1. Forward current flow through the junction gives Lambertian spontaneous emission and the device emits light from all surfaces. However, only a limited amount of light

escapes the structure due to total internal reflection, and therefore the radiance is low.

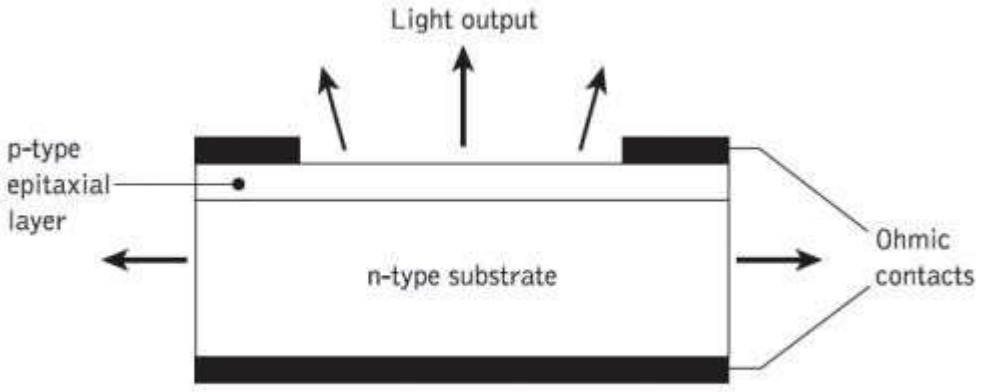

Figure 3.1 The structure of a planar LED showing the emission of light from all surfaces

[Source: htpp://img.brainkart.com]

The absence of optical amplification through stimulated emission in the LED tends to limit the internal quantum efficiency (ratio of photons generated to injected electrons) of the device. Reliance on spontaneous emission allows non-radiative recombination to take place within the structure due to crystalline imperfections and impurities giving, at best, an internal quantum efficiency of 50% for simple homojunction devices. However, as with injection lasers, double-heterojunction (DH) structures have been implemented which recombination lifetime measurements suggest give internal quantum efficiencies of 60 to 80%.

The power generated internally by an LED may be determined by consideration of the excess electrons and holes in the *p*- and *n*-type material respectively (i.e. the minority carriers) when it is forward biased and carrier injection takes place at the device contacts. The excess density of electrons n and holes p is equal since the injected carriers are created and recombined in pairs such that charge neutrality is maintained within the structure.

LED STRUCTURES

1. Surface Emitting LEDs

A method for obtaining high radiance is to restrict the emission to a small active region within the device. The technique pioneered by Burrus and Dawson with homostructure devices was to use an etched well in a GaAs substrate in order to prevent heavy absorption of the emitted radiation, and physically to accommodate the fiber. These structures have a low thermal impedance in the active region allowing high current densities and giving high-radiance emission into the optical fiber. Furthermore, considerable advantage may be obtained by employing DH structures giving increased efficiency from electrical and optical confinement as well as less absorption of the emitted radiation.

This type of surface emitter LED (SLED) has been widely employed within optical fiber communications. The structure of a high-radiance etched well DH surface emitter* for the 0.8 to 0.9μm wavelength band is shown in Figure 3.2. The internal absorption in this device is very low due to the larger bandgap-confining layers, and the reflection coefficient at the back crystal face is high giving good forward radiance. The emission from the active layer is essentially isotropic, although the external emission distribution may be considered Lambertian with a beam width of 120° due to refraction from a high to a low refractive index at the GaAs–fiber interface. The power coupled *P*c into a multimode step index fiber may be estimated from the relationship:

$$P_c = \pi (1 - r) A R_D (NA)^2 \qquad (3.1)$$

where *r* is the Fresnel reflection coefficient at the fiber surface, *A* is the smaller of the fiber core cross-section or the emission area of the source and *R*D is the radiance of the source.

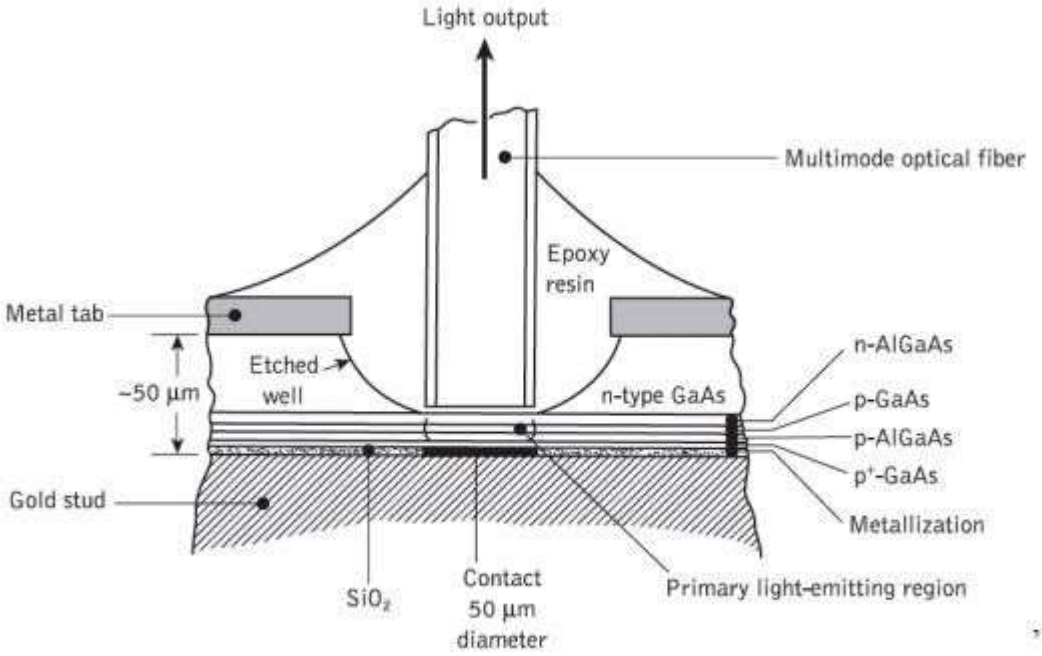

Figure 3.2 The structure of an AlGaAs DH surface-emitting LED (Burrus type).

[Source: htpp://img.brainkart.com]

However, the power coupled into the fiber is also dependent on many other factors including the distance and alignment between the emission area and the fiber, the SLED emission pattern and the medium between the emitting area and the fiber. For instance, the addition of epoxy resin in the etched well tends to reduce the refractive index mismatch and increase the external power efficiency of the device. Hence, DH surface emitters often give more coupled optical power than predicted by Eq. (3.1).

However, for graded index fiber optimum direct coupling requires that the source diameter be about one-half the fiber core diameter. In both cases lens coupling may give increased levels of optical power coupled into the fiber but at the cost of additional complexity. Other factors which complicate the LED fiber coupling are the transmission characteristics of the leaky modes or large angle skew rays. Much of the optical power from an incoherent source is initially

coupled into these large-angle rays, which fall within the acceptance angle of the fiber but have much higher energy than meridional rays. Energy from these rays goes into the cladding and may be lost.

Hence much of the light coupled into a multimode fiber from an LED is lost within a few hundred meters. It must therefore be noted that the effective optical power coupled into a short length of fiber significantly exceeds that coupled into a longer length. The planar structure of the Burrus-type LED and other nonetched well SLEDs allows significant lateral current spreading, particularly for contact diameters less than 25 μm. This current spreading results in a reduced current density as well as an effective emission area substantially greater than the contact area.

2. Edge Emitting LEDs

Another basic high-radiance structure currently used in optical communications is the stripe geometry DH edge emitter LED (ELED). This device has a similar geometry to a conventional contact stripe injection laser, as shown in Figure 3.3. It takes advantage of transparent guiding layers with a very thin active layer (50 to 100 μm) in order that the light produced in the active layer spreads into the transparent guiding layers, reducing self-absorption in the active layer. The consequent waveguiding narrows the beam divergence to a half-power width of around 30° in the plane perpendicular to the junction. However, the lack of waveguiding in the plane of the junction gives a Lambertian output with a half-power width of around 120°, as illustrated in Figure3.3.

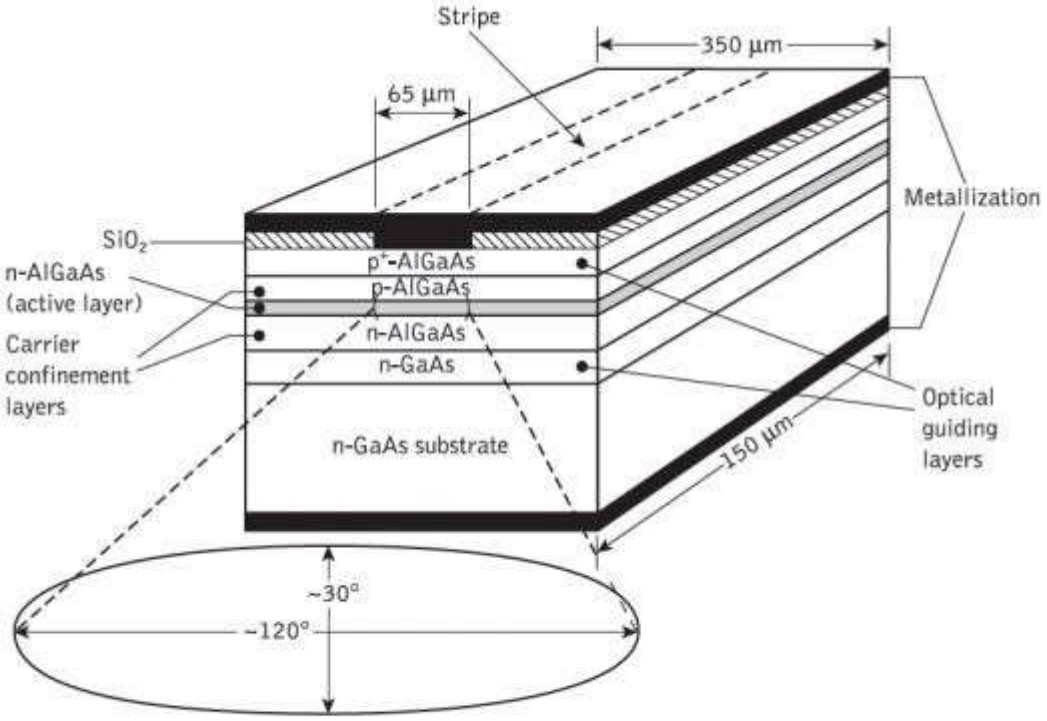

Figure 3.3 Schematic illustration of the structure of a stripe geometry DH AlGaAs edge-emitting LED

[Source: htpp://img.brainkart.com]

Most of the propagating light is emitted at one end face only due to a reflector on the other end face and an antireflection coating on the emitting end face. The effective radiance at the emitting end face can be very high giving an increased coupling efficiency into small-*NA* fiber compared with the surface emitter. However, surface emitters generally radiate more power into air (2.5 to 3 times) than edge emitters since the emitted light is less affected by reabsorption and interfacial recombination. Comparisons have shown that edge emitters couple more optical power into low *NA* (less than 0.3) than surface emitters, whereas the opposite is true for large *NA* (greater than 0.3).

The enhanced waveguiding of the edge emitter enables it in theory to couple 7.5 times more power into low-*NA* fiber than a comparable surface emitter. However, in practice the increased coupling efficiency has been found

to be slightly less than this (3.5 to 6 times). Similar coupling efficiencies may be achieved into low-*NA* fiber with surface emitters by the use of a lens. Furthermore, it has been found that lens coupling with edge emitters may increase the coupling efficiencies by comparable factors (around five times).

The stripe geometry of the edge emitter allows very high carrier injection densities for given drive currents. Thus it is possible to couple approaching a milliwatt of optical power into low-*NA* (0.14) multimode step index fiber with edge-emitting LEDs operating at high drive currents (500 mA).

Edge emitters have also been found to have a substantially better modulation bandwidth of the order of hundreds of megahertz than comparable surface-emitting structures with the same drive level. In general it is possible to construct edge-emitting LEDs with a narrower linewidth than surface emitters, but there are manufacturing problems with the more complicated structure (including difficult heat-sinking geometry) which moderate the benefits of these devices.

Optical Detectors

The basic detection process in an intrinsic absorber is illustrated in Figure 3.11 which shows a *p*–*n* photodiode. This device is reverse biased and the electric field developed across the *p*–*n* junction sweeps mobile carriers (holes and electrons) to their respective majority sides (*p*- and *n*-type material). A depletion region or layer is therefore created on either side of the junction. This barrier has the effect of stopping the majority carriers crossing the junction in the opposite direction to the field. However, the field accelerates minority carriers from both sides to the opposite side of the junction, forming the reverse leakage current of the diode. Thus intrinsic conditions are created in the depletion region.

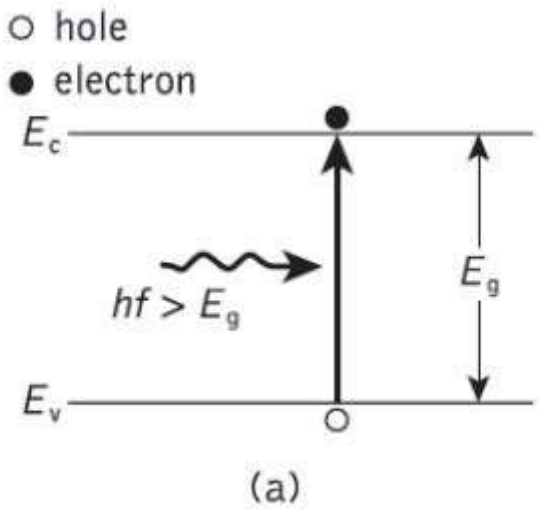

(a)

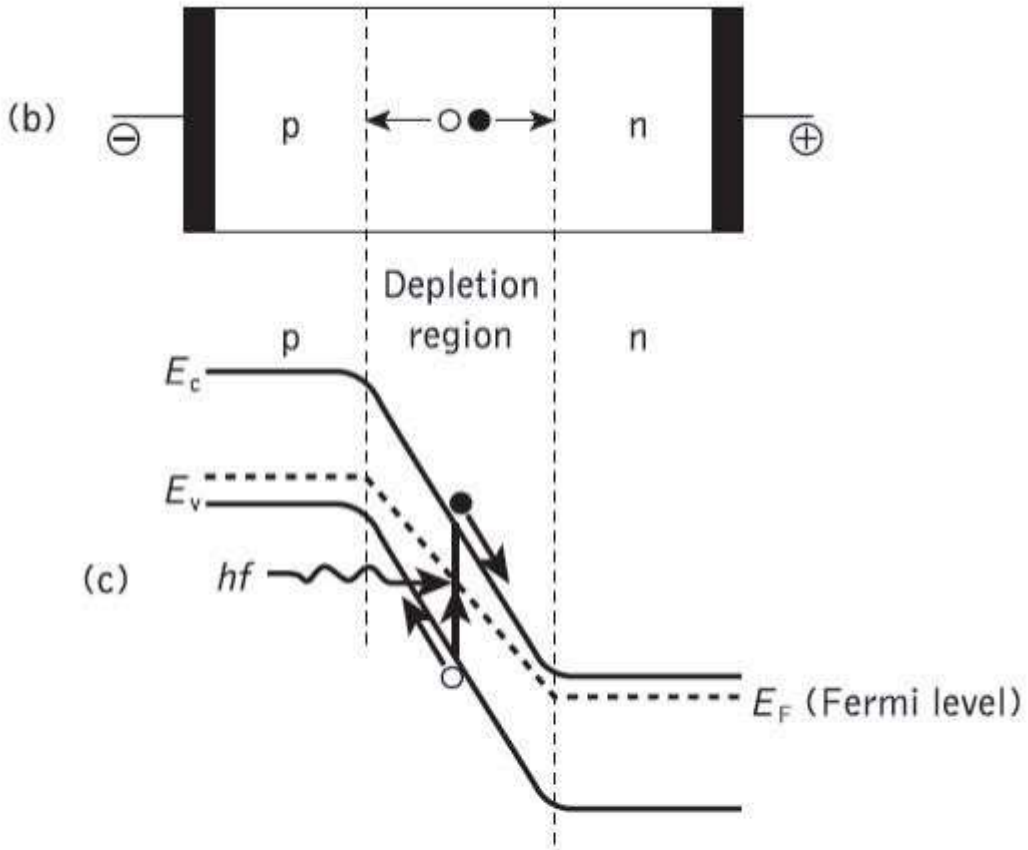

Figure 3.11 Operation of the *p–n* photodiode: (a) photogeneration of an electron–hole pair in an intrinsic semiconductor; (b) the structure of the reverse-biased *p–n* junction illustrating carrier drift in the depletion region; (c) the energy band diagram of the reverse-biased *p–n* junction showing photogeneration and the subsequent separation of an electron–hole pair

[Source: htpp://img.brainkart.com]

1. PIN Photo Detectors

In order to allow operation at longer wavelengths where the light penetrates more deeply into the semiconductor material, a wider depletion region is necessary. To achieve this then-type material is doped so lightly that it can be considered intrinsic, and to make a low resistance contact a highly doped *n*-type (n+) layer is added. This creates a *p–i–n* (or PIN) structure, as may be seen in Figure 3.12 where all the absorption takes place in the depletion region.

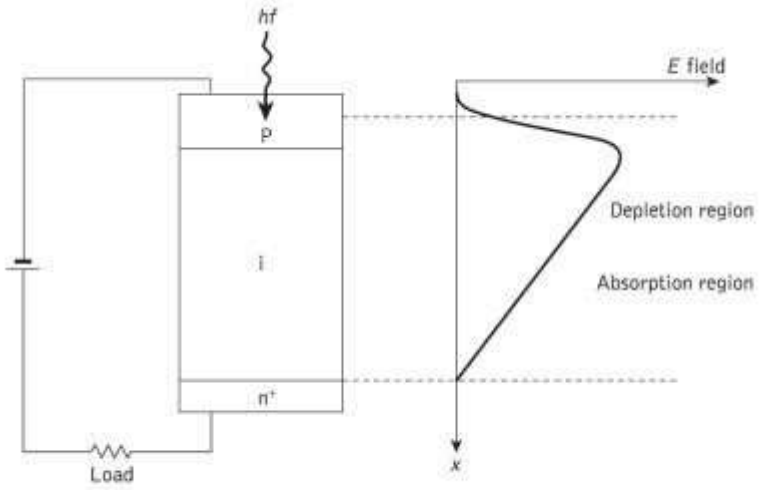

Figure 3.12 The *p–i–n* photodiode showing the combined absorption and depletion region

[Source: htpp://img.brainkart.com]

Figure 3.13 shows the structures of two types of silicon *p–i–n* photodiode for operation in the shorter wavelength band below 1.09 μm. The front-illuminated photodiode, when operating in the 0.8 to 0.9 μm band (Figure 3.13(a)), requires a depletion region of between 20 and 50 μm in order to attain high quantum efficiency (typically 85%) together with fast response (less than 1 ns) and low dark current (1 nA). Dark current arises from surface leakage currents as well as generation– recombination currents in the depletion region in the absence of illumination.

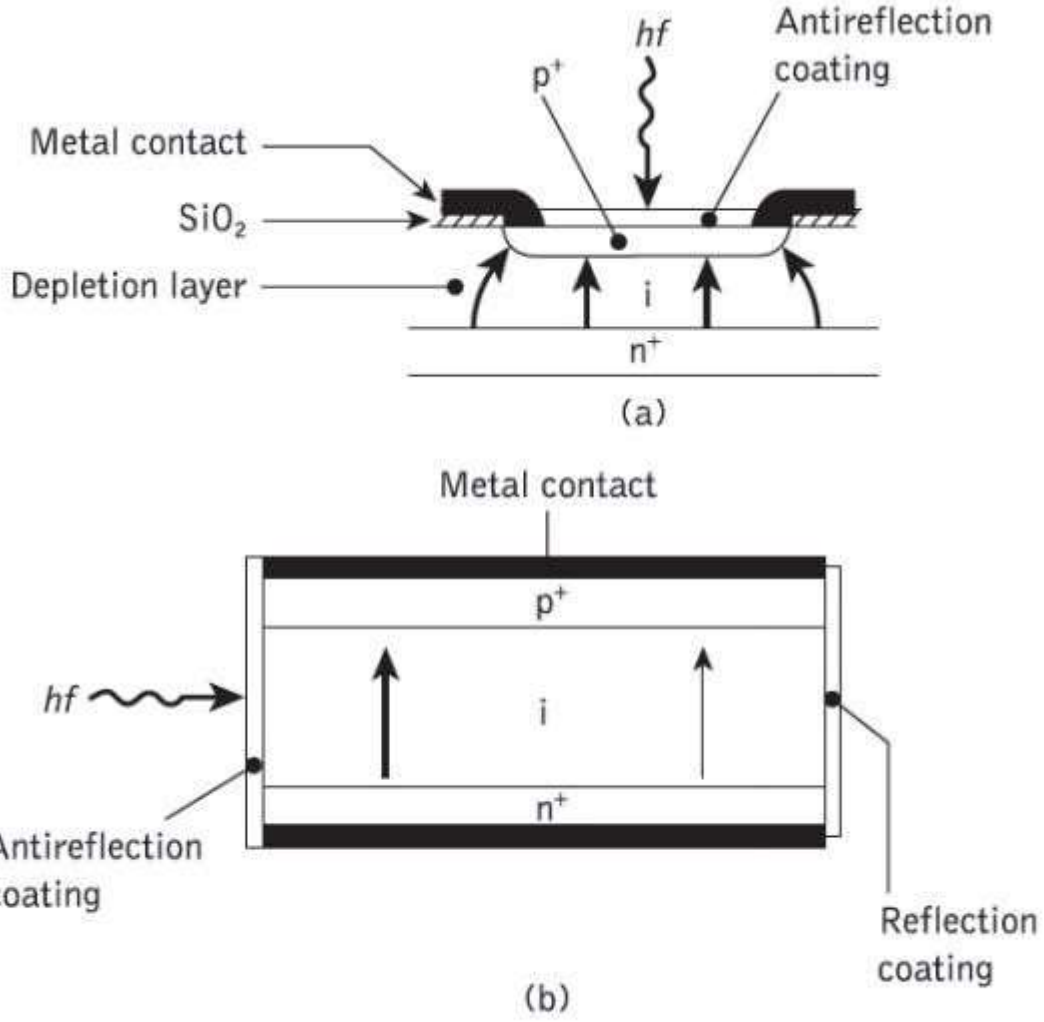

Figure 3.13 (a) Structure of a front-illuminated silicon *p–i–n* photodiode. (b) Structure of a side-illuminated (parallel to junction) *p–i–n* photodiode

[Source: htpp://img.brainkart.com]

The side-illuminated structure (Figure 3.13(b)), where light is injected parallel to the junction plane, exhibits a large absorption width (_500 μm) and hence is particularly sensitive at wavelengths close to the bandgap limit (1.09 μm) where the absorption coefficient is relatively small. Germanium *p–i–n* photodiodes which span the entire wavelength range of interest are also commercially available, but as mentioned previously the relatively high dark currents are a problem (typically 100 nA at 20 °C increasing to 1 μA at 40 °C).

The favoured material is the lattice-matched In0.53Ga0.47As/InP system which can detect at wavelengths up to 1.67 μm. A typical planar device structure is shown in Figure 3.14(a) which requires epitaxial growth of several layers on an *n*-type InP substrate. The incident light is absorbed in the low-doped *n*-type InGaAs layer generating carriers, as illustrated in the energy band diagram Figure 3.14(b). The discontinuity due to the homojunction between the n+-InP substrate and the n-InGaAs absorption region may be noted. This can be reduced by the incorporation of an *n*-type InP buffer layer.

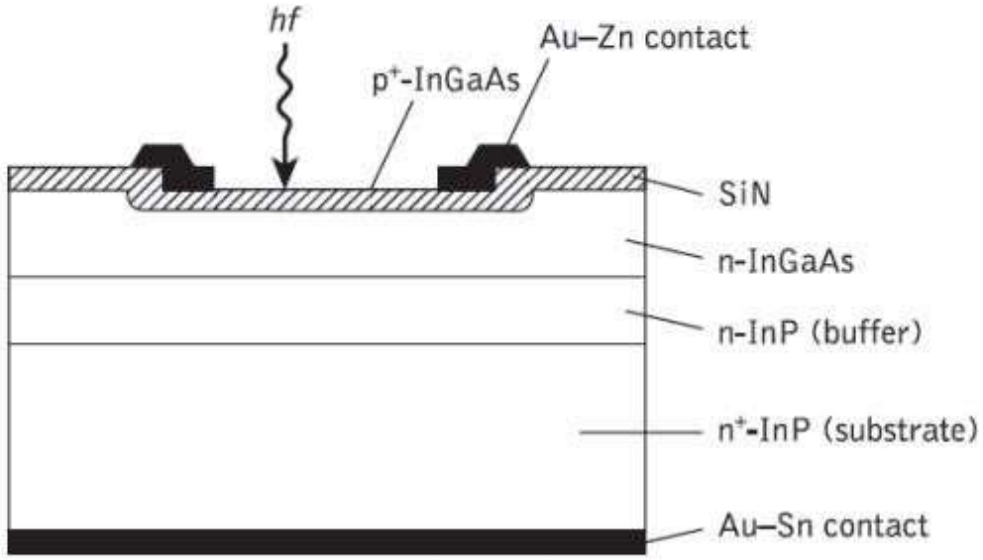

(a)

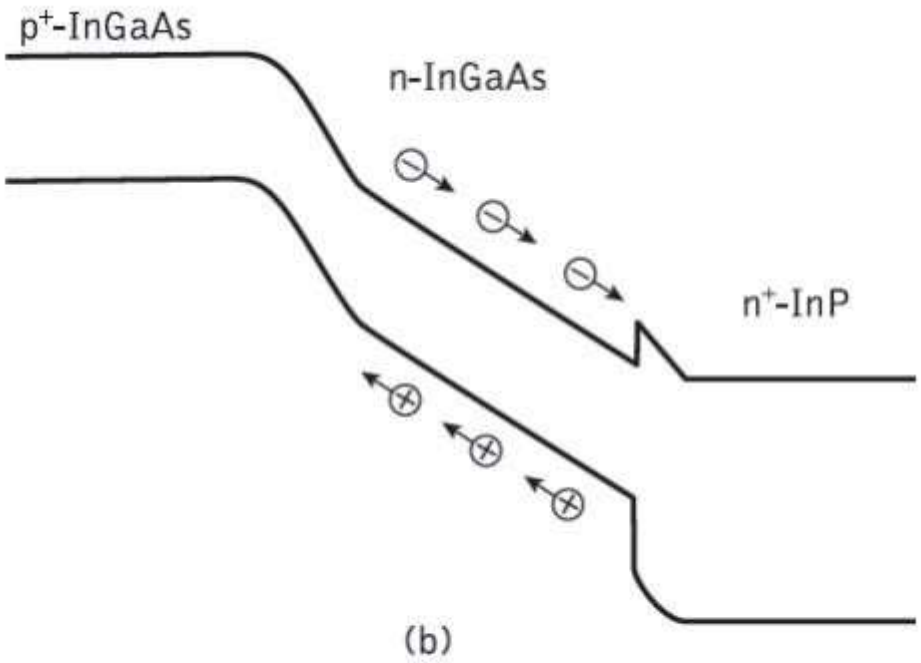

Figure 3.14 Planar InGaAs *p–i–n* photodiode: (a) structure; (b) energy band diagram showing homojunction associated with the conventional *p–i–n* structure

[Source: htpp://img.brainkart.com]

The top entry* device shown in Figure 3.14(a) is the simplest structure, with the light being introduced through the upper p+-layer. However, a drawback with this structure is a quantum efficiency penalty which results from optical absorption in the undepleted p+- region. In addition, there is a limit to how small such a device can be fabricated as both light access and metallic contact are required on the top. To enable smaller devices with lower capacitances to be made, a substrate entry technique is employed. In this case light enters through a transparent InP substrate and the device area can be fabricated as small as may be practical for bonding.

2. Avalanche Photodiodes

The second major type of optical communications detector is the avalanche photodiode (APD). This has a more sophisticated structure than the *p–i–n* photodiode in order to create an extremely high electric field region

(approximately 3 × 105 V cm−1), as may be seen in Figure 3.15(a). Therefore, as well as the depletion region where most of the photons are absorbed and the primary carrier pairs generated, there is a high-field region in which holes and electrons can acquire sufficient energy to excite new electron–hole pairs.

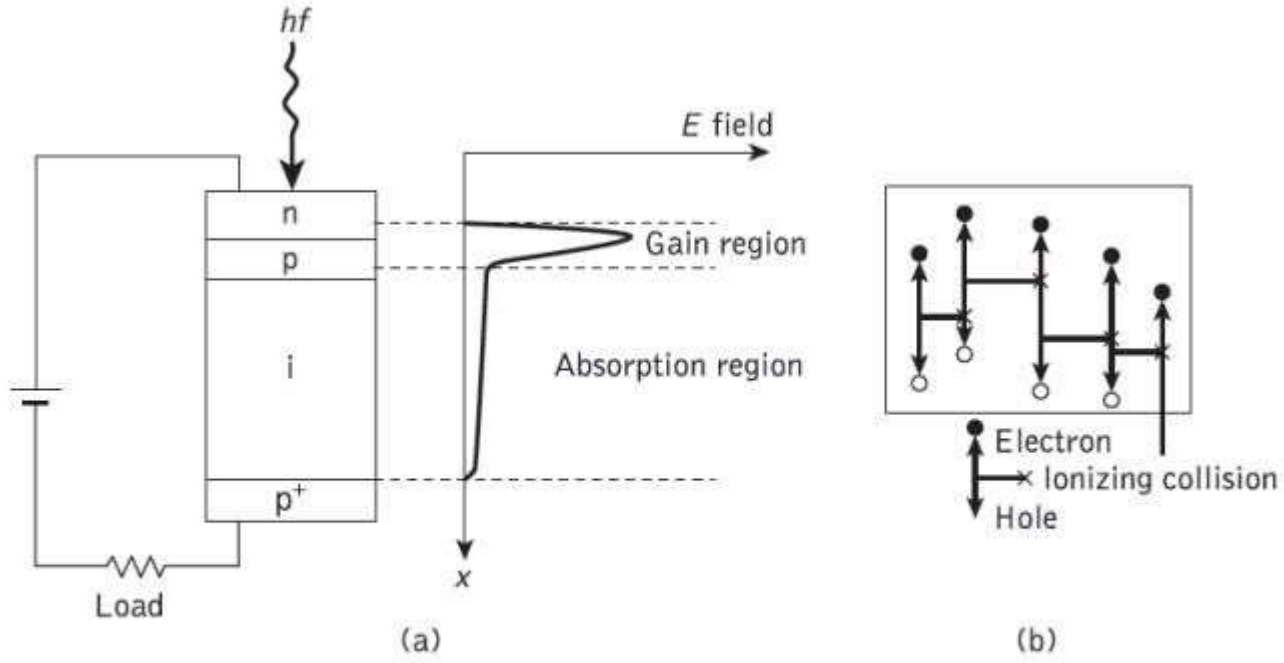

Figure 3.15 (a) Avalanche photodiode showing high electric field (gain) region. (b) Carrier pair multiplication in the gain region of an avalanche photodiode

[Source: htpp://img.brainkart.com]

This process is known as impact ionization and is the phenomenon that leads to avalanche breakdown in ordinary reverse-biased diodes. It often requires high reverse bias voltages (50 to 400 V) in order that the new carriers created by impact ionization can themselves produce additional carriers by the same mechanism as shown in Figure 3.15(b). More recently, however, it should be noted that devices which will operate at much lower bias voltages (15 to 25 V) have become available.

Carrier multiplication factors as great as 104 may be obtained using defect-free materials to ensure uniformity of carrier multiplication over the entire photosensitive area. However, other factors affect the achievement of high gain within the device. Micro plasmas, which are small areas with lower breakdown

voltages than the remainder of the junction, must be reduced through the selection of defect-free materials together with careful device processing and fabrication.

In addition, excessive leakage at the junction edges can be eliminated by the use of a guard ring structure as shown in Figure 3.16. At present silicon, germanium and InGaAs APDs are generally available.Operation of these devices at high speed requires full depletion in the absorption region. When carriers are generated in undepleted material, they are collected somewhat slowly by the diffusion process. This has the effect of producing a long ‘diffusion tail’ on a short optical pulse. When the APD is fully depleted by employing electric fields in excess of 104 Vm−1, all the carriers drift at saturation-limited velocities. In this case the response time for the device is limited by three factors.

These are:

(a)the transit time of the carriers across the absorption region (i.e. the depletion width)

(b) the time taken by the carriers to perform the avalanche multiplication process

(c) and the *RC* time constant incurred by the junction capacitance of the diode and its load.

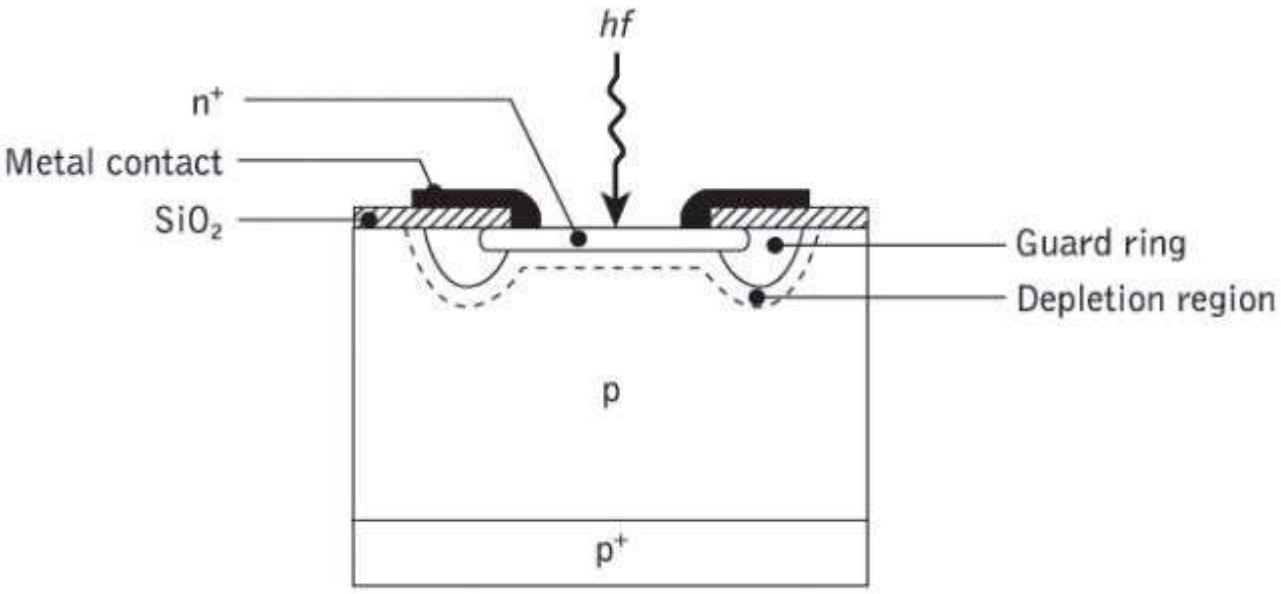

Figure 8.16 Structure of a silicon avalanche photodiode (APD) with guard ring

[Source: htpp://img.brainkart.com]

At low gain the transit time and *RC* effects dominate giving a definitive response time and hence constant bandwidth for the device. However, at high gain the avalanche build up time dominates and therefore the device bandwidth decreases proportionately with increasing gain. Such APD operation is distinguished by a constant gain–bandwidth product. Often an asymmetric pulse shape is obtained from the APD which results from a relatively fast rise time as the electrons are collected and a fall time dictated by the transit time of the holes traveling at a slower speed. Hence, although the use of suitable materials and structures may give rise times between 150 and 200 ps, fall times of 1 ns or more are quite common and limit the overall response of the device.

Photo detector Noise & S/N Ratio Calculation:

Detection of weak optical signal requires that the photodetector and its following amplification circuitry be optimized for a desired signal-to-noise ratio.

It is the noise current which determines the minimum optical power level that can be detected. This minimum detectable optical power defines the **sensitivity** of photo detector. That is the optical power that generates a photocurrent with the amplitude equal to that of the total noise current (*S/N=1*)

$$\frac{S}{N} = \frac{\text{signal power from photocurrent}}{\text{photodetector noise power} + \text{amplifier noise power}}$$

1. Signal Calculation:

Consider the modulated optical power signal *P(t)* falls on the photodetector with the form of

$$P(t) = P_0[1 + ms(t)]$$

Where *s(t)* is message electrical signal and *m* is modulation index. Therefore the primary photocurrent is (for pin photodiode *M=1*):

$$i_{ph} = \frac{\eta q}{h\nu} MP(t) = I_p[\text{DC value}] + i_p(t)[\text{AC current}]$$

The root mean square signal current is then

$$\langle i_s^2 \rangle = \langle i_p^2 \rangle M^2 = \sigma_s^2$$

$$\langle i_p^2 \rangle = \sigma_p^2 = \frac{m^2 I_P^2}{2} \quad \text{for sinusoidal signal}$$

Noise Sources in Photo detectors:

The principal noises associated with photo detectors are:

1- Quantum (Shot) noise: arises from statistical nature of the production and collection of photo-generated electrons upon optical illumination. It has been shown that the statistics follow a Poisson process.

2- Dark current noise: is the current that continues to flow through the bias circuit in the absence of the light. This is the combination of bulk dark current, which is due to thermally generated e and h in the *pn* junction, and the surface dark current, due to surface defects, bias voltage an surface area.

- In order to calculate the total noise presented in photodetector, we should sum up the root mean square of each noise current by assuming that those are uncorrelated.
- Total photo detector noise current=quantum noise current +bulk dark current noise + surface current noise

Noise calculation:

Quantum noise current (lower limit on the sensitivity):

$$\langle i_Q^2 \rangle = \sigma_Q^2 = 2qI_P BM^2 F(M)$$

B: Bandwidth, $F(M)$ is the noise figure and generally is

$$F(M) \approx M^x \quad 0 \le x \le 1.0$$

Bulk dark current noise:

$$\langle i_{DB}^2 \rangle = \sigma_{DB}^2 = 2qI_D BM^2 F(M)$$

Surface dark current noise

$$\langle i_{DS}^2 \rangle = \sigma_{DS}^2 = 2qI_L B$$

The total rms photodetector noise current is:

$$\langle i_N^2 \rangle = \sigma_N^2 = \langle i_Q^2 \rangle + \langle i_{DB}^2 \rangle + \langle i_{DS}^2 \rangle$$
$$= 2q(I_P + I_D) BM^2 F(M) + 2qI_L B$$

The thermal noise of amplifier connected to the photodetector is:

$$\langle i_T^2 \rangle = \sigma_T^2 = \frac{4k_B TB}{R_L}$$

2. S/N Calculation:

Having obtained the signal and total noise, the signal-to-noise-ratio can be written as:

$$\frac{S}{N} = \frac{\langle i_P^2 \rangle M^2}{2q(I_P + I_D) BM^2 F(M) + 2qI_L B + 4k_B TB/R_L}$$

Since the noise figure *F(M)* increases with M, there always exists an optimum value of *M* that maximizes the S/N. For sinusoidally modulated signal with *m=1* and *F*(*M*) = *Mx*

$$M_{\text{opt}}^{x+2} = \frac{2qI_L + 4k_B T / R_L}{xq(I_P + I_D)}$$

Photodetector Response Time

The response time of a photodetector with its output circuit depends mainly on the following three factors:

1- The transit time of the photocarriers in the depletion region. The transit time depends on the carrier drift velocity and the depletion layer width *w*, and is given by:

$$t_d = \frac{W}{v_d}$$

2- Diffusion time of photocarriers outside depletion region.

3- *RC* time constant of the circuit

$$B = \frac{1}{2\pi R_T C_T}$$

$$R_T = R_s \parallel R_L \text{ and } C_T = C_a + C_d$$